INTERNATIONAL JOURNAL FOR NUMERICAL METHODS IN FLUIDS
Int. J. Numer. Meth. Fluids 2003; **43**:1221–1238 (DOI: 10.1002/fld.507)

Low dissipative high-order numerical simulations of supersonic reactive flows

Björn Sjögreen[1,*,†,‡] and H. C. Yee[2]

[1]*Royal Institute of Technology, NADA, Stockholm 100 44, Sweden*
[2]*NASA Ames Research Centre, Moffett Field, CA 94035, U.S.A.*

SUMMARY

We report the performance of a newly developed low dissipative sixth-order spatial and fourth-order temporal scheme (*J. Comput. Phys.* 1999; **150**:199; *RIACS Report* 01.01, NASA Ames Research Centre, October 2000) for multiscale supersonic reactive flows that contain shock waves. The accuracy and efficiency of the scheme are compared with a low-dissipative fifth-order weighted ENO (WENO) scheme (*ICASE Report No.* 95-73, 1995). This paper confirms and complements the grid convergence study of Sjögreen and Yee where a complex shock/shear/boundary-layer interactions model was also included.

A 2D viscous flow consisting of a planar Mach 2 in air interacting with a circular zone of hydrogen bubbles in two different initial configurations is considered. The two initial configurations are a single bubble and two non-aligned bubbles. The gradient in pressure across the shock in conjunction with the gradient in fluid density between the air and hydrogen produce a large increase in vorticity as the shock passes through the hydrogen fuel. As can be seen in the study of Don and Quillen (*J. Comput. Phys.* 1995; **122**:244), Don and Gottlieb (*SIAM J. Numer. Anal.* 1998; **35**:2370) and the present grid convergence study, the size, spacing and velocity of the fine-scale vortical structures are very difficult to accurately simulate numerically. The difficulty in obtaining well-resolved multiscale combustion flows by all methods considered will be illustrated. Published in 2003 by John Wiley & Sons, Ltd.

KEY WORDS: high-order finite-difference method; shock waves; supersonic combustion

1. INTRODUCTION

In the modelling of viscous problems containing finite-rate chemistry, a wide range of space and timescales is often present, over and above the different scales associated with turbulence flows, leading to additional numerical difficulties. This stems mainly from the fact that most numerical algorithms used in reacting flows were originally designed to solve non-reacting

* Correspondence to: B. Sjögreen, Royal Institute of Technology, NADA, 100 44 Stockholm, Sweden.
† E-mail: bjorns@nada.kth.se
‡ Part of this work was carried out while the first author was a visiting scientist with the Research Institute of Advanced Computer Science (RIACS), NASA Ames Research Centre. RIACS Technical Report 01.17, May 2001.

Contract/grant sponsor: COSMO

Received 17 October 2002
Revised 12 December 2002

fluid flows. It was shown in Reference [1] that, for stiff reactions containing shock waves, it is possible to obtain stable solutions that look reasonable and yet are completely wrong, because the discontinuities are in the wrong locations. Largely due to numerical dissipation, stiff reaction waves move at non-physical wave speeds, often at the rate of one grid cell per time step, regardless of their proper speed. There exist several methods that can overcome this difficulty for a single reaction term. For more than a single reacting term in fully coupled non-linear systems, more research is needed. One impractical way of minimizing the wrong speed of propagation of discontinuities is to demand orders of magnitude grid size reduction compared with what appears to be a reasonable grid spacing in practice. Another way is to develop efficient, stable, non-dissipative or very low-dissipative adaptive high accurate schemes.

Based on fixed time step and grid spacing analysis, it was also shown in References [2, 3] that the numerical phenomenon of incorrect propagation speeds of discontinuities may be linked to the existence of some stable spurious steady–state numerical solutions, and that the various ways of discretizing the reaction term can affect the stability of the overall scheme. Pointwise evaluation of the source terms appears to be the least stable. In addition, it was shown in References [4, 5] (also based on fixed time step and grid spacing analysis) that spurious discrete travelling waves can exist, depending on the method of discretizing the source term. When physical diffusion is added, it is not known what type of numerical difficulties will surface. Appropriate adaptive time step and adaptive grid spacing controls can alleviate some of the spurious behaviour at the expense of higher computational cost, complexity in programming and added unknown non-linearity effects introduced into the overall computational system. At present, efficient and reliable dynamics grid adaptation schemes for rapidly developing multiscale complex viscous flows are not fully developed. Guidelines in numerical treatment of source terms (other than pointwise evaluation) for highly coupled non-linear systems are not available. This paper focuses only on the numerical dissipation issue. The degree of improvement in resolution of fine scale flow structures by the sixth-order low dissipative method over standard second-order TVD methods is examined.

The outline of the paper is as follows. Section 2 gives a brief description of the numerical methods. Detailed formulation of the scheme can be found in References [6, 7]. The unsteady supersonic combustion model is given in Section 3 together with the numerical results for the two test problems. Section 4 discusses the computer implementation.

2. NUMERICAL METHODS

In the Yee *et al.* [6, 8] method, one time step consists of one step with a fourth-order or higher accurate non-dissipative spatial base scheme along with a post-processing step, where regions of oscillation are detected using an artificial compression method (ACM) [3] sensor, and the solution is filtered by adding the numerical dissipation portion of a shock capturing scheme in these regions. Often an entropy split form of the inviscid flux derivative [8–10] is used. The entropy splitting of the inviscid flux derivative is considered as a conditioned (or more stable) form of the governing equations. The idea of the scheme is to have the spatially high-order accurate non-dissipative scheme activated at all times and to add the full strength, efficient and accurate numerical dissipation only at the shock layers. Thus, it is necessary to have good detectors which flag the layers, and not the oscillatory turbulent parts of the flow

field. Entropy splitting is built in as an option in our computer code. For strong shocks, the gain in stability by using the entropy splitting is diminished. See Reference [8] for a study. Since the two chosen model problems contain strong viscous shocks, the entropy splitting is not used for the inviscid fluxes for the computations reported here. Successful examples of the benefit of entropy splitting on flows with long time wave propagations, low speed compressible turbulence and/or weak shocks are shown in References [8, 11].

It was shown in Yee *et al.* that the ACM sensor, while minimizing the use of numerical dissipation away from discontinuities, requires tuning parameters and is physical problem dependent. To minimize the tuning of parameters and physical problem dependence, new sensors with improved detection properties were proposed in Reference [7]. The new sensors are derived by utilizing appropriate non-orthogonal wavelet basis functions and can be used to completely switch off the extra numerical dissipation outside shock layers. The non-dissipative spatial base scheme of arbitrarily high-order of accuracy can be maintained without compromising its stability at all parts of the domain where the solution is smooth. Two types of redundant non-orthogonal wavelet basis functions are considered. One is the B-spline wavelet [12] used by Gerritsen and Olsson [10] in an adaptive mesh refinement method to determine regions where refinement should be done. The other is a modification of the multiresolution method of Harten [13] by converting it to a new, redundant, non-orthogonal wavelet. The wavelet sensor is then obtained by computing the estimated Lipschitz exponent of a chosen physical quantity (or vector) to be sensed on a chosen wavelet basis function. Both wavelet sensors can be viewed as dual purpose adaptive methods leading to dynamic numerical dissipation control and improved grid adaptation indicators. Consequently, they are useful not only for shock-turbulence computations but also for chemical reaction and combustion simulations.

For all of the computations, central differencing is used for the viscous terms with the order matching the order of the base scheme for the inviscid fluxes. For the reacting terms, pointwise evaluation of the source terms is adopted. That is, the source terms are evaluated at the grid point (j,k). Although pointwise evaluation of the source terms appears to be the least stable procedure for inviscid flows [2, 3], when physical diffusion is present, no known guidelines are available.

These two high-order filter schemes are hereafter referred to as the ACM and wavelet filter schemes. This filter approach is particularly important for multiscale viscous flows. The procedure takes the physical viscosity and the reacting terms into consideration since only non-dissipative high-order schemes are used as the base scheme. In other words, numerical dissipation based on the convection terms is used to filter the numerical solution at the completion of the full step of the time integration, and only at regions where the physical viscosity is inadequate to stabilize the high frequency oscillations due to the non-dissipative nature of the base scheme.

We use the same notation as in References [6, 8, 14]. The ACM and wavelet filter schemes with sixth-order central base scheme for both the inviscid and viscous flux derivatives are denoted by ACM66 and WAV66. See References [6, 8, 14] for the forms of these filter schemes. The scheme using the fifth-order WENO for the inviscid flux derivatives and sixth-order central for viscous flux derivatives is denoted by WENO5. For the ACM66, WAV66 and WENO5, the standard fourth-order Runge–Kutta temporal discretization is employed. We denote these schemes as ACM66-RK4, WAV66-RK4 and WENO5-RK4. Except WENO5-RK4, the rest of the methods, unless otherwise indicated, use the Roe's average state and the van Leer limiter for the numerical dissipation portion of the filter. The wavelet decomposition

was applied in density and pressure, and the maximum wavelet coefficient of the two components was used. The numerical dissipation is switched on wherever the wavelet analysis gives a Lipschitz exponent less than 0.5. Increasing this number will reduce oscillations, at the price of reduced accuracy. See Reference [7] for other possibilities.

The WENO5 is implemented as described in Reference [15] with the only difference being that we use the classical fourth-order Runge–Kutta method in time (WENO5-RK4). The WENO5 method is a discretization of the convective terms using a weighted average of third-order accurate finite-difference stencils. The stencils are applied in characteristic variables, and are biased in the upwind direction. The weights in the averaging are constructed such that stencils over non-smooth regions are weighted out, and such that the method becomes fifth-order accurate when the solution is smooth. We used global Lax–Friedrichs fluxes as the basis for the WENO method.

3. A SUPERSONIC COMBUSTION MODEL

For the numerical experiment, the same supersonic reactive flow problem concerning fuel breakup and mixing of different configurations as presented in References [16, 17] is used. This is a simplified model that might be used as fuel mixing in advanced aerospace propulsion systems, e.g. a hydrogen fuel supersonic combustion scramjet that is capable of propelling a space vehicle at hypersonic speed. See Reference [17] and references cited therein for a discussion.

The governing equations are the compressible Navier–Stokes equations with four species undergoing multichemical reactions. The equations are formulated in the conserved variables $\mathbf{U}=(\rho_1,\ldots,\rho_N,\rho u,\rho v,e)$, where ρ is the density of the mixture, (u,v) are velocities, and e is the total energy. $\rho_i=\rho y_i$, where y_i is the mass fraction of species i. The equations are in the form

$$\mathbf{U}_t+\mathbf{F}_x(\mathbf{U})+\mathbf{G}_y(\mathbf{U})=\mathbf{F}_x^v(\mathbf{U},\mathbf{U}_x,\mathbf{U}_y)+\mathbf{G}_y^v(\mathbf{U},\mathbf{U}_x,\mathbf{U}_y)+\mathbf{S}(\mathbf{W})$$

with standard convective flux vectors $\mathbf{F}$ and $\mathbf{G}$, and diffusive flux vectors $\mathbf{F}^v$ and $\mathbf{G}^v$. $\mathbf{S}(\mathbf{W})$ is the source term representing chemical reactions.

Total energy is modelled as

$$e=\sum_{i=1}^{N}\rho_i\varepsilon_i(T)+\frac{1}{2}\rho u^2+\sum_{i=1}^{N}h_i^0\rho_i$$

where the internal energy $\varepsilon_i(T)$ is computed by a polynomial fit to thermodynamical data. The formation enthalpies, h_i^0, are given numbers. Sutherland's law,

$$\mu_i=\mu_0^i\left(\frac{T}{T_0^i}\right)^{3/2}\left(\frac{T_0^i+S^i}{T+S^i}\right)$$

is used to model the viscosity of each species. μ_0^i, T_0^i, S^i are constants, different for different species. The total viscosity of the mixture is computed from Wilke's law,

$$\mu=\sum_{i=1}^{N}\frac{\mu_i X_i}{\sum_{j=1}^{N}X_j\phi_{ij}}$$

where

$$\phi_{ij} = \frac{(1 + ((\mu_i/\mu_j)(y_j/y_i))^{1/2}(M_i/M_j)^{1/4})^2}{(8(1 + M_i/M_j))^{1/2}}$$

and X_i are molar fractions, and M_i is the molar mass of species i. A Prandtl number, $Pr = 0.72$, Schmidt number $Sc = 0.22$, and the perfect gas equation of state approximation are used. The mixture specific heat at constant pressure was obtained from McBride *et al.* [18]. The Svehla [19] species viscosity constants and the Wilke's law model [20] for the mixture viscosity are used.

The chemical reaction is modelled by a single-step reversible reaction using H_2, O_2, H_2O and N_2. The single-step reversible reaction using H_2, O_2, H_2O and N_2 is

$$2H_2 + O_2 \rightleftharpoons 2H_2O$$

Species N_2 is inert. See Don and Gottlieb for detailed discussion of the model.

A 2D flow consisting of a planar shock in air interacting with a circular zone of hydrogen bubbles in two different initial configurations is considered. The two initial configurations are (a) a single bubble and (b) two non-aligned bubbles. The temperature of the hydrogen and air in the undisturbed region ahead of the shock is set to 1000°K with a pressure of 1 atm. and zero velocity. A Mach 2 shock is placed at $x_s = 0.005$. The gradient in pressure across the shock in conjunction with the gradient in fluid density between the air and hydrogen produces a large increase in vorticity as the shock passes through the hydrogen fuel. As can be seen in the numerical simulation of Don and Quillen, and Don and Gottlieb using spectral and high-order ENO schemes, and the present grid convergence study, the size, spacing and velocity of the fine-scale vortical structures are very difficult to accurately simulate numerically.

The reason for choosing this particular problem, was that it is well known, and well documented in the literature. Several high-order solutions can be found, for example in References [16, 17].

3.1. Planar shock interacting with a single hydrogen bubble

In the first test problem a planar shock in air is interacting with a single circular hydrogen bubble. The radius of the hydrogen bubble is 0.01. A Mach 2 shock is placed at $x_s = 0.005$. The domain is $0 \leqslant x \leqslant 0.175$ and $-0.045 \leqslant y \leqslant 0.045$. All of the computations use uniform Cartesian grid spacing as was done by Don and Quillen and Don and Gottlieb. Figure 1 shows snapshots of the density at six different stages of the evolutionary process, computed by ACM66-RK4 using a 500×250 grid. The shock breaks the bubble into two smaller hydrogen bubbles. These bubbles start to rotate after the shock has passed through, and a complex structure develops inside the bubbles. In Figure 2, we show a convergence study at time 60 μs, illustrated by the hydrogen mass fraction using the second-order Runge–Kutta temporal discretization and the spatial second-order TVD scheme of Harten and Yee (TVD-RK2) using the minmod limiter. For this study we only compute on the domain $0 \leqslant x \leqslant 0.09$ and $0 \leqslant y \leqslant 0.045$. Symmetry conditions are enforced on the lower boundary.

Results from TVD66-RK4, ACM66-RK4, WAV66-RK4 and WENO5-RK4 methods are shown in Figures 3–6. We also show, in Figure 2, results from using the second-order Harten–Yee TVD scheme, which is a more standard state of the art solution technique. Here TVD66-RK4 differs from ACM66-RK4 in that the ACM sensor is set to 1. The grid dimension are

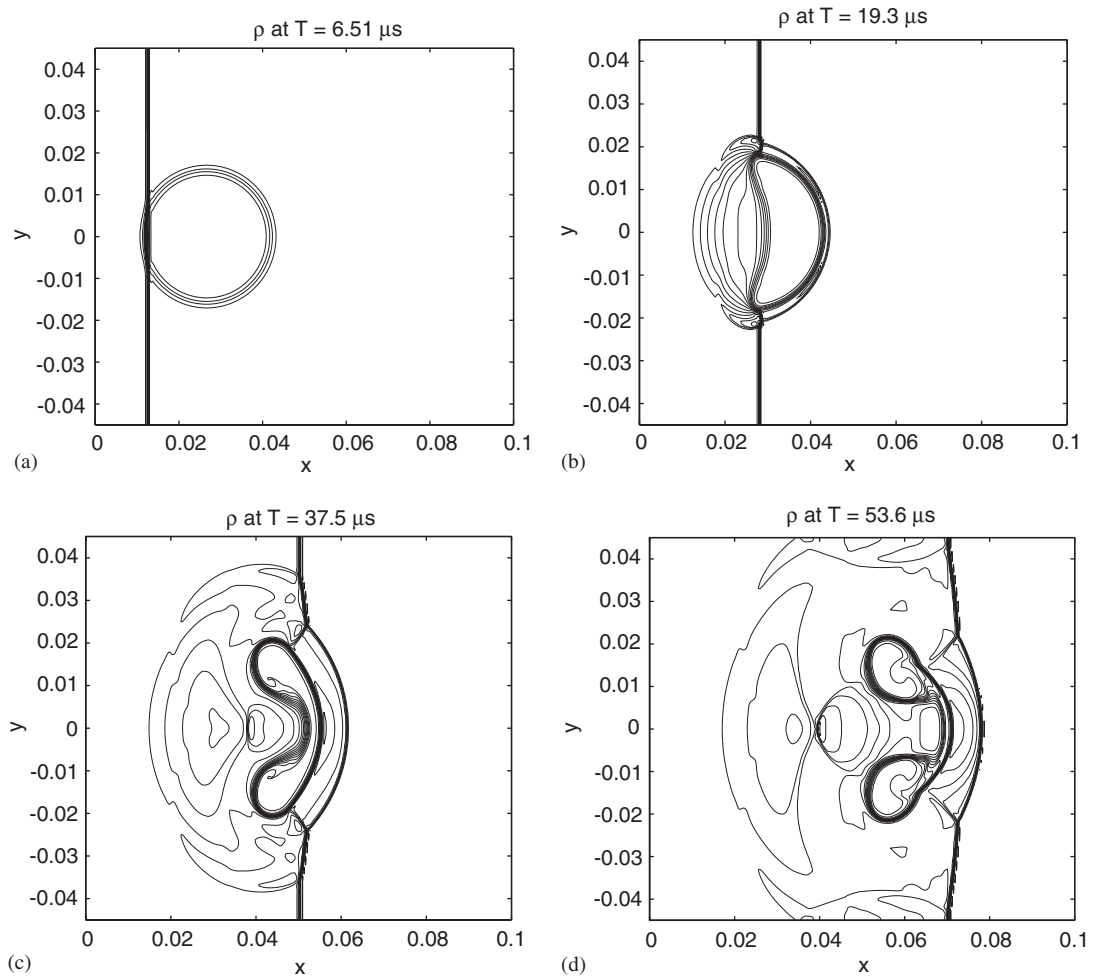

Figure 1. Density contours of ACM66-RK4 on a 500×250 grid: Time evolution of a Mach 2 shock in air interacting with one hydrogen bubble: (a) Time 6.51 μs. (b) Time 19.31 μs. (c) Time 37.5 μs. (d) Time 53.6 μs.

increased from 250×125 to 4000×2000 for some schemes. One can see the advantage of the ACM sensor by examining the two solutions. The results using ACM66-RK4 are less diffusive than those using TVD66-RK4. It seems that WENO5-RK4 gives a solution which is similar to the solution obtained by the TVD-RK2 on a grid which is one level finer. The flow structures and convergence trends from the ACM66-RK4 and TVD66-RK4 are similar. Grid convergence of the fine-scale flow structures are not perfectly reached with either method. At approximately 2000×1000 grid points the global structure of the solutions have reached the regime where the viscous, parabolic part of the operator starts to have significant influence on the explicit time step from the CFL condition. For coarser grids we see that the WENO5-RK4 scheme gives a resolution which is similar to that of TVD66 and is somewhat more

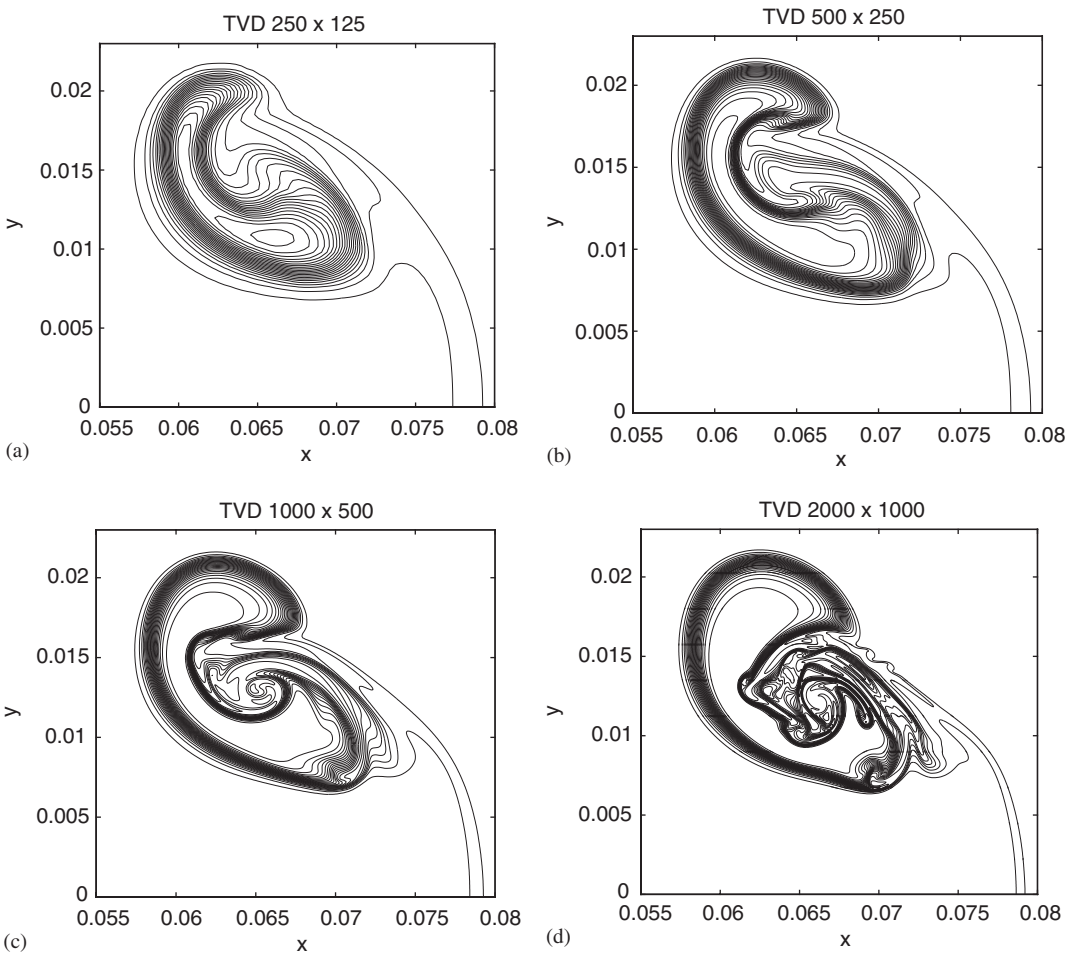

Figure 2. Grid refinement of the second-order Harten–Yee TVD scheme (TVD-RK2). Hydrogen mass fraction contours at time 60 μs: (a) TVD-RK2, 250×125 grid. (b) TVD-RK2, 500×250 grid. (c) TVD-RK2, 1000×500 grid. (d) TVD-RK2, 2000×1000 grid.

diffuse than that of ACM66. The fine scale solution structures depart from the two methods as we refine the grid. The CPU per time step by WENO5-RK4 is 2.5 times of the rest of the schemes which are similar in CPU. Therefore, computations beyond a 1000×500 grid using WENO5-RK4 are too time consuming and costly.

There are two CFL conditions used here, one for the fluid ($\mathrm{CFL} = 0.6$) and one for the reacting terms ($\mathrm{CFL} = 0.3$). The values 0.6 and 0.3 turned out to work well in practice. We only tried a few values. It would perhaps be possible to find somewhat larger values that work well, too. The two CFL conditions give two different time steps. The smallest of these two time steps is used. For this model and the above grid convergence study, it is difficult to assess the exact accuracy and robustness of these schemes. Since the structure develops rapidly, static grid adaptations might not be practical and dynamic grid adaptations are still

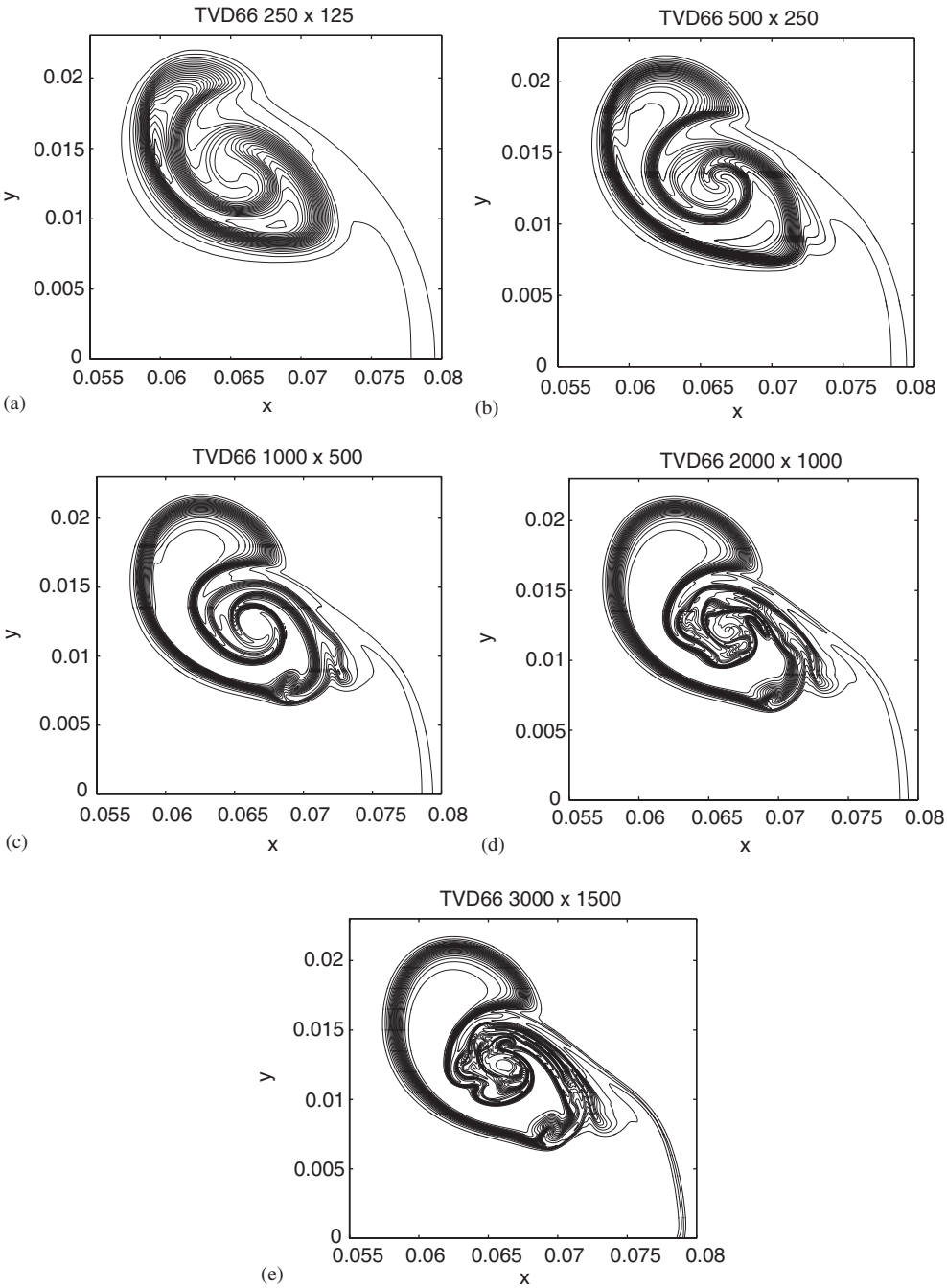

Figure 3. Grid refinement of the TVD66-RK4 scheme. Hydrogen mass fraction contours at time 60 μs: (a) TVD66-RK4, 250×125 grid. (b) TVD66-RK4, 500×250 grid. (c) TVD66-RK4, 1000×500 grid. (d) TVD66-RK4, 2000×1000 grid. (e) TVD66-RK4, 3000×1500 grid.

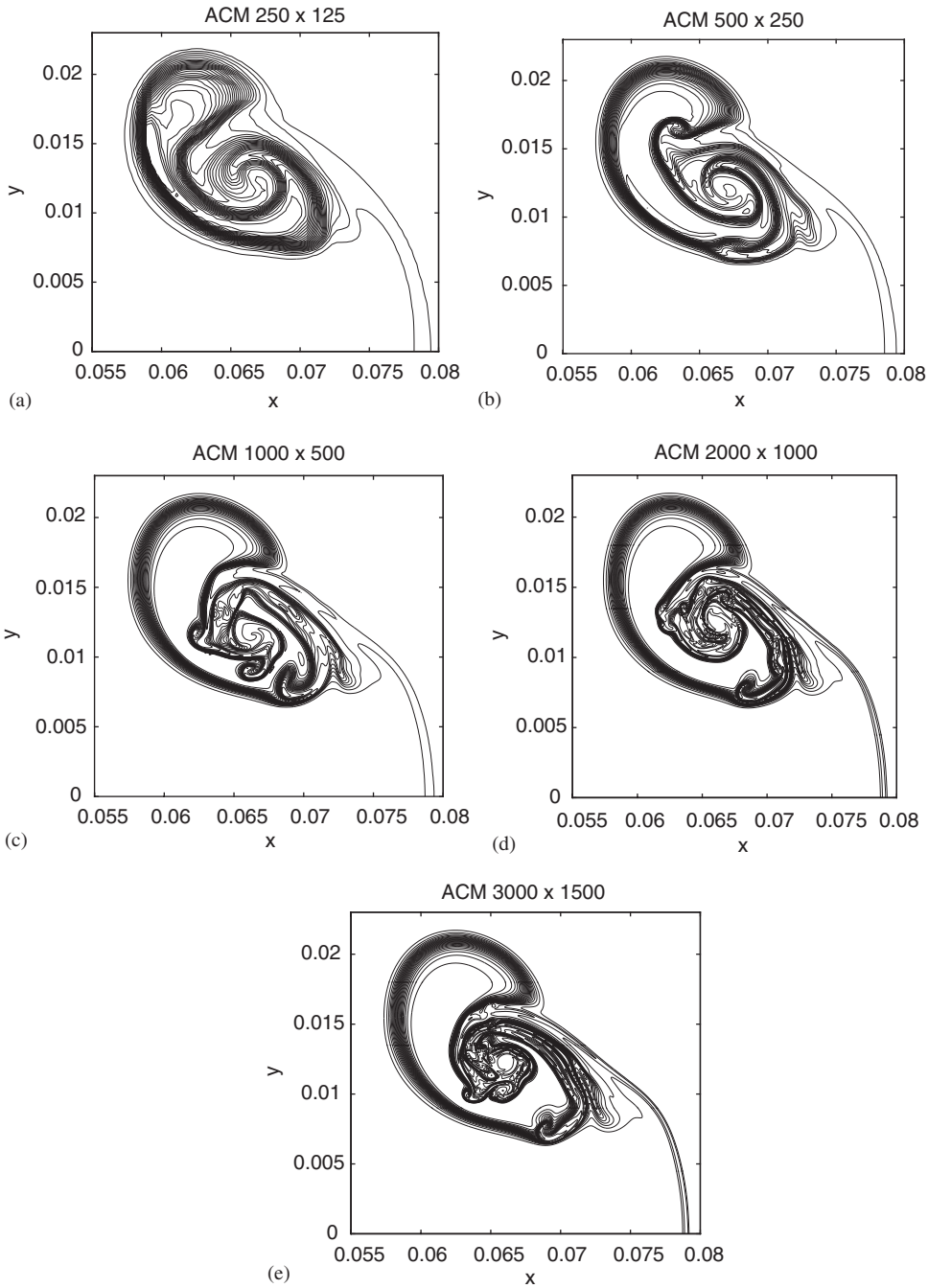

Figure 4. Grid refinement of the ACM66-RK4 scheme. Hydrogen mass fraction contours at time 60 μs: (a) ACM66-RK4, 250 × 125 grid. (b) ACM66-RK4, 500 × 250 grid. (c) ACM66-RK4, 1000 × 500 grid. (d) ACM66-RK4, 2000 × 1000 grid. (e) ACM66-RK4, 3000 × 1500 grid.

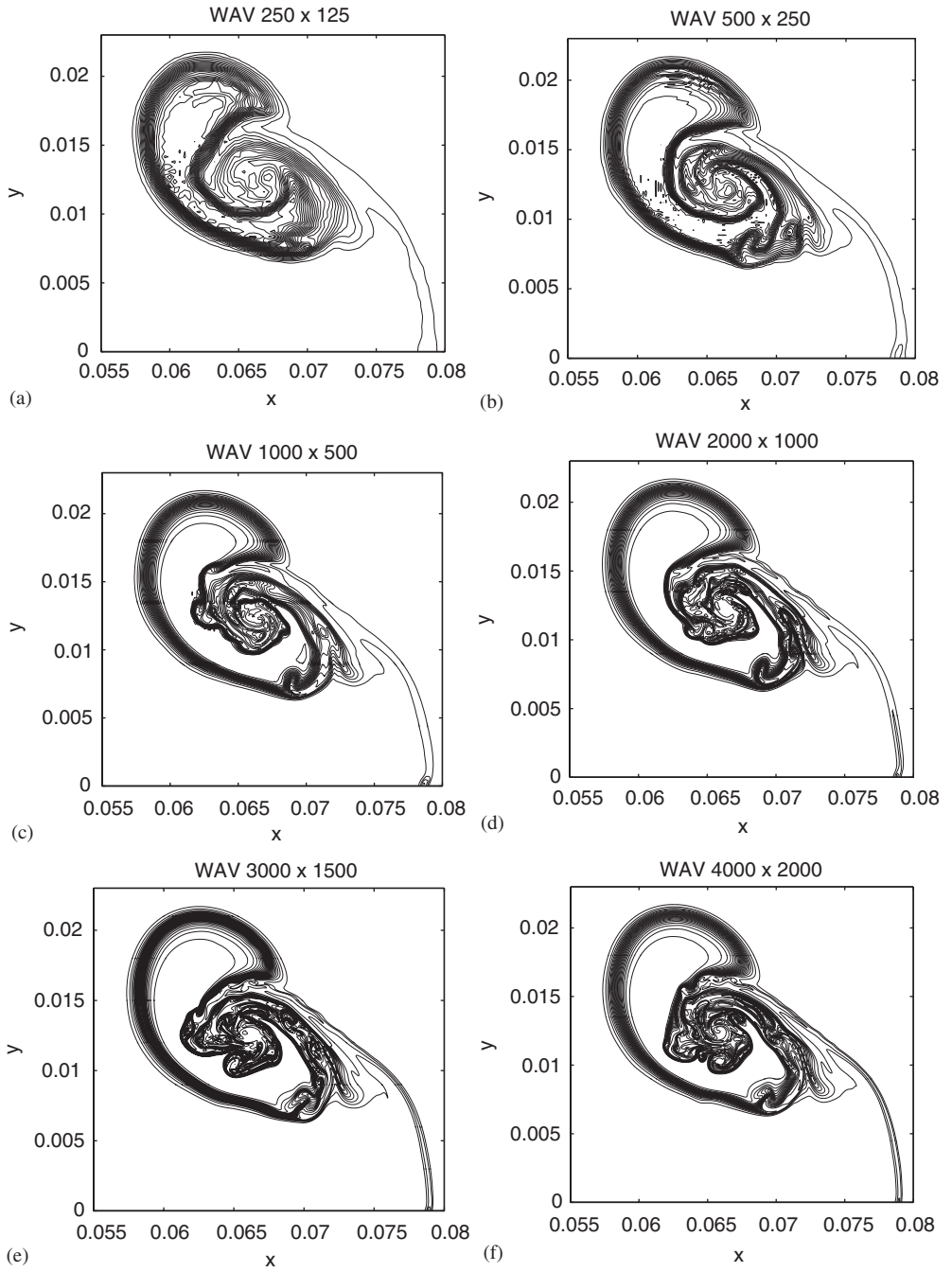

Figure 5. Grid refinement of the WAV66-RK4 scheme. Hydrogen mass fraction contours at time 60 μs: (a) WAV66-RK4, 250×125 grid. (b) WAV66-RK4, 500×250 grid. (c) WAV66-RK4, 1000×500 grid. (d) WAV66-RK4, 2000×1000 grid. (e) WAV66-RK4, 3000×1500 grid. (f) WAV66-RK4, 4000×2000 grid.

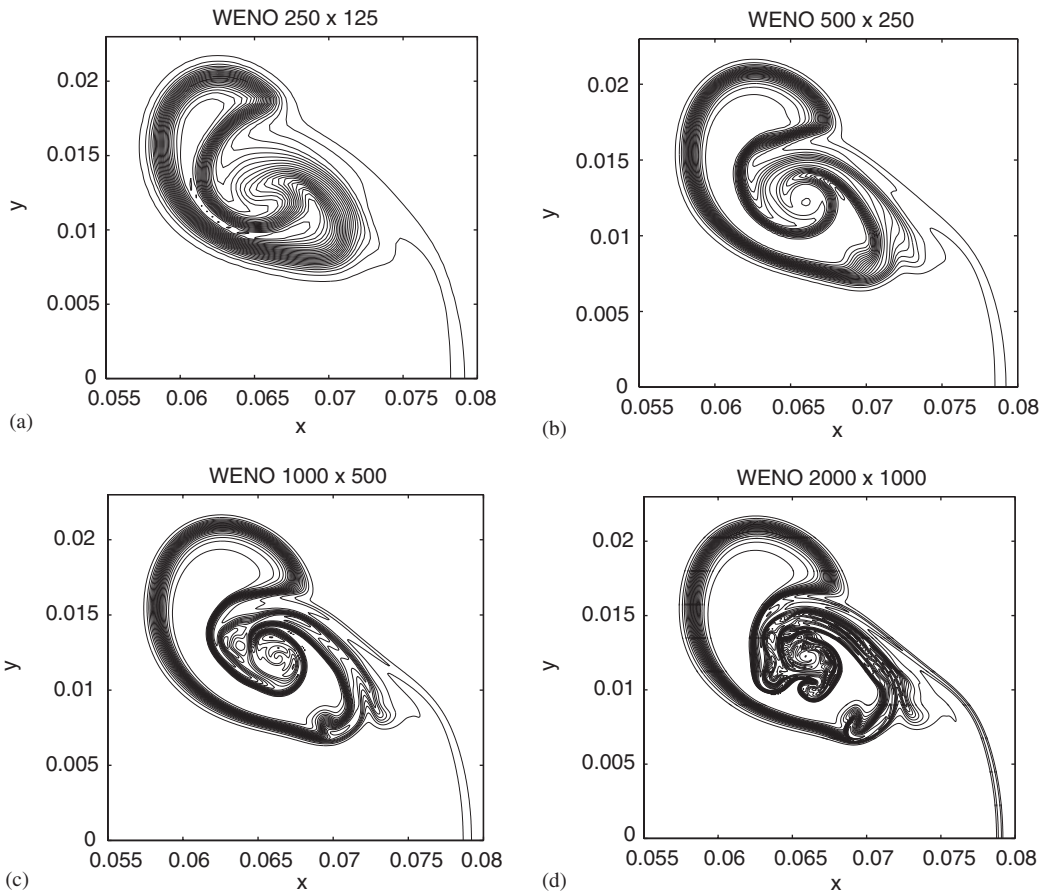

Figure 6. Grid refinement of the WENO5-RK4 scheme. Hydrogen mass fraction contours at time 60 μs: (a) WENO5-RK4, 250×125 grid. (b) WENO5-RK4, 500×250 grid. (c) WENO5-RK4, 1000×500 grid. (d) WENO5-RK4, 2000×1000 grid.

under development. The results reported here reveal the challenge of obtaining well-resolved multiscale complex flow structures of reactive and/or combustion problems without the use of an efficient and reliable dynamic grid adaptation procedure.

3.2. Planar shock interacting with two hydrogen bubbles

As a second test problem we solve the above equations with initial data consisting of two non-aligned circular hydrogen bubbles. The first is centred at $(0.0275, 0.01)$ and the second at $(0.0675, -0.01)$. They both have radius 0.02. We compute on a domain $0 \leqslant x \leqslant 0.18$, and $-0.045 \leqslant y \leqslant 0.045$. Snapshots of the density contours at six different stages of the evolutionary process computed by ACM66-RK4 using a 500×250 grid are shown in Figure 7. The asymmetric nature of the initial data causes the hydrogen bubbles to split up into smaller pieces. The flow pattern is very complicated. For details see Reference [17].

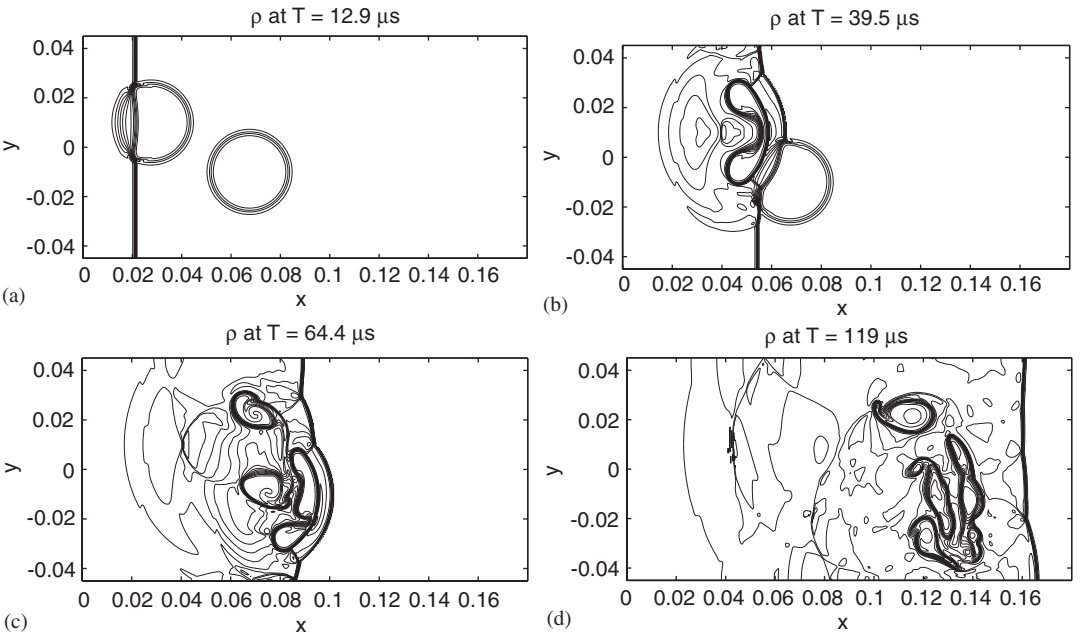

Figure 7. Density contours by ACM66-RK4, using a 500×250 grid. Time evolution of a planar Mach 2 shock in air interacting with two initially non-aligned circular hydrogen bubbles: (a) Time 12.9 μs. (b) Time 39.5 μs. (c) Time 64.4 μs. (d) Time 119 μs.

We study the grid convergence for the solution at time 125 μs. In Figure 8, we show results from using the TVD-RK2. The same computation with ACM66-RK4, WAV66-RK4 and WENO5-RK4 are shown in Figures 9–11. These figures indicate that the sixth-order methods give better resolution on coarser grids than the low-order methods. The grid dimensions are increased from 250×125 to 4000×2000 for some schemes. The wavelet filter scheme gives by far the best resolution of small-scale features. Using similar grid sizes as the one bubble case, grid convergence was difficult to reach. The fine-scale structure inside the hydrogen bubbles was not resolved unless a very refined grid was used. As seen in Figure 10, the WAV66-RK4 solution appears to change very little between the 3000×1500 and 4000×2000 refinement, and we believe that grid convergence is reached at 4000×2000 grid points. Study for example the small tip at $x = 0.15$, $y = -0.01$, which is clearly visible on the two finest grids of the WAV66-RK4 solution. This structure is not present at any of the solutions on coarser grids.

In practice we cannot afford to use a grid with several thousand points in each coordinate direction. Assume, for example, that we can afford to solve the problem on a grid of 500×250 points. Assume that the exact solution is close to the 4000×2000 points WAV66-RK4 solution. Comparing Figures 8–11, at the resolution 500×250 points, we conclude that the WENO5-RK4 is superior to the standard method TVD-RK2, but that the sixth-order accurate ACM66-RK4 and WAV66-RK4 give even better representation of small scales.

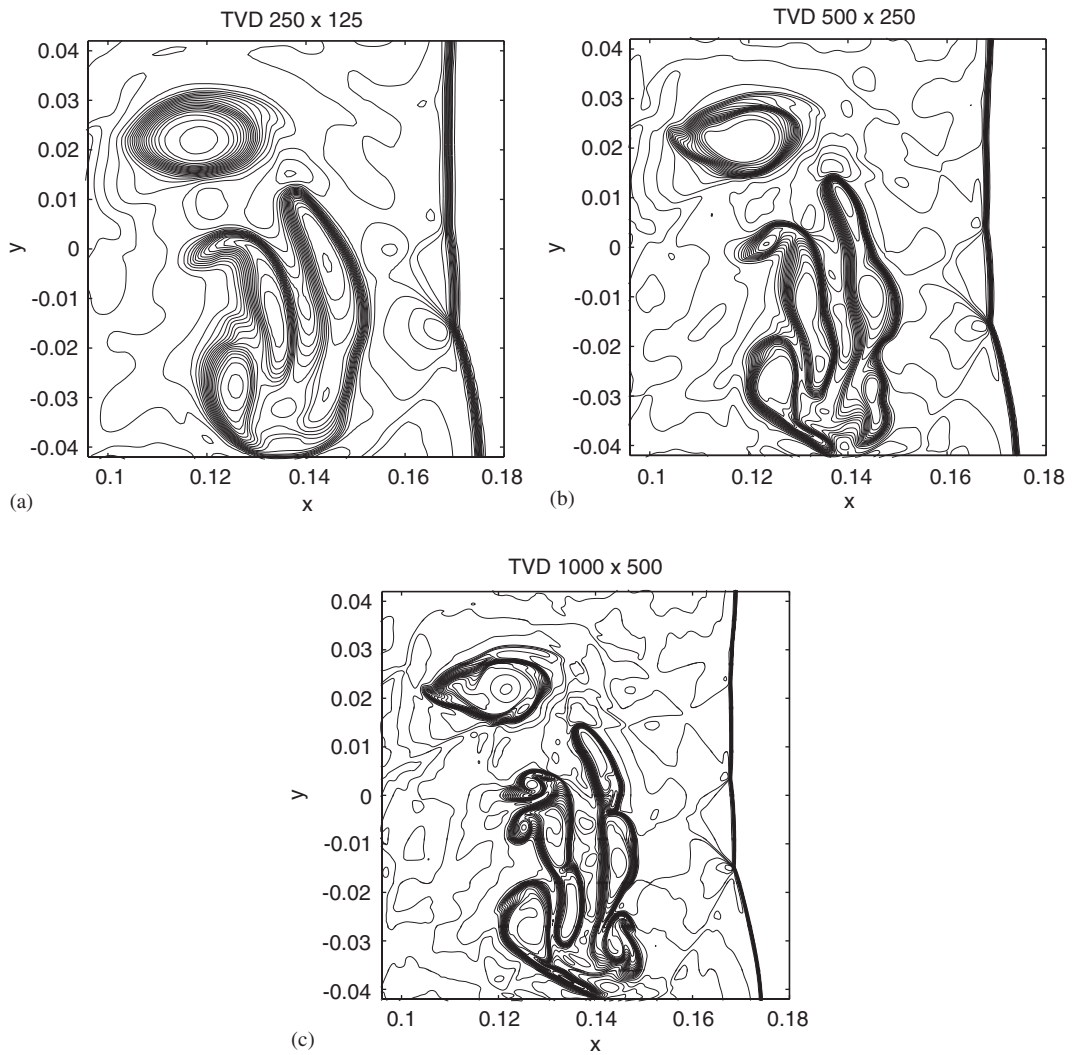

Figure 8. Grid refinement of second-order Harten–Yee TVD scheme TVD-RK2: Density contours at time 125 μs of a planar shock interacting with two initially non-aligned circular hydrogen bubbles: (a) TVD-RK2, 250×125 grid. (b) TVD-RK2, 500×250 grid. (c) TVD-RK2, 1000×500 grid.

4. COMPUTER IMPLEMENTATION

The computations presented here would not have been possible without use of high performance supercomputers. Most of the computations were done on a 512 processor SGI Origin2000 at NASA Ames Research Centre. Some computations were done on a 300 processor IBM/SP2 at the Centre for Parallel Computers (PDC) in Stockholm, Sweden. Our code is parallelized using the Message Passing Interface (MPI) library. The code automatically divides the computational domain into equal sized patches. Sufficient overlap of points

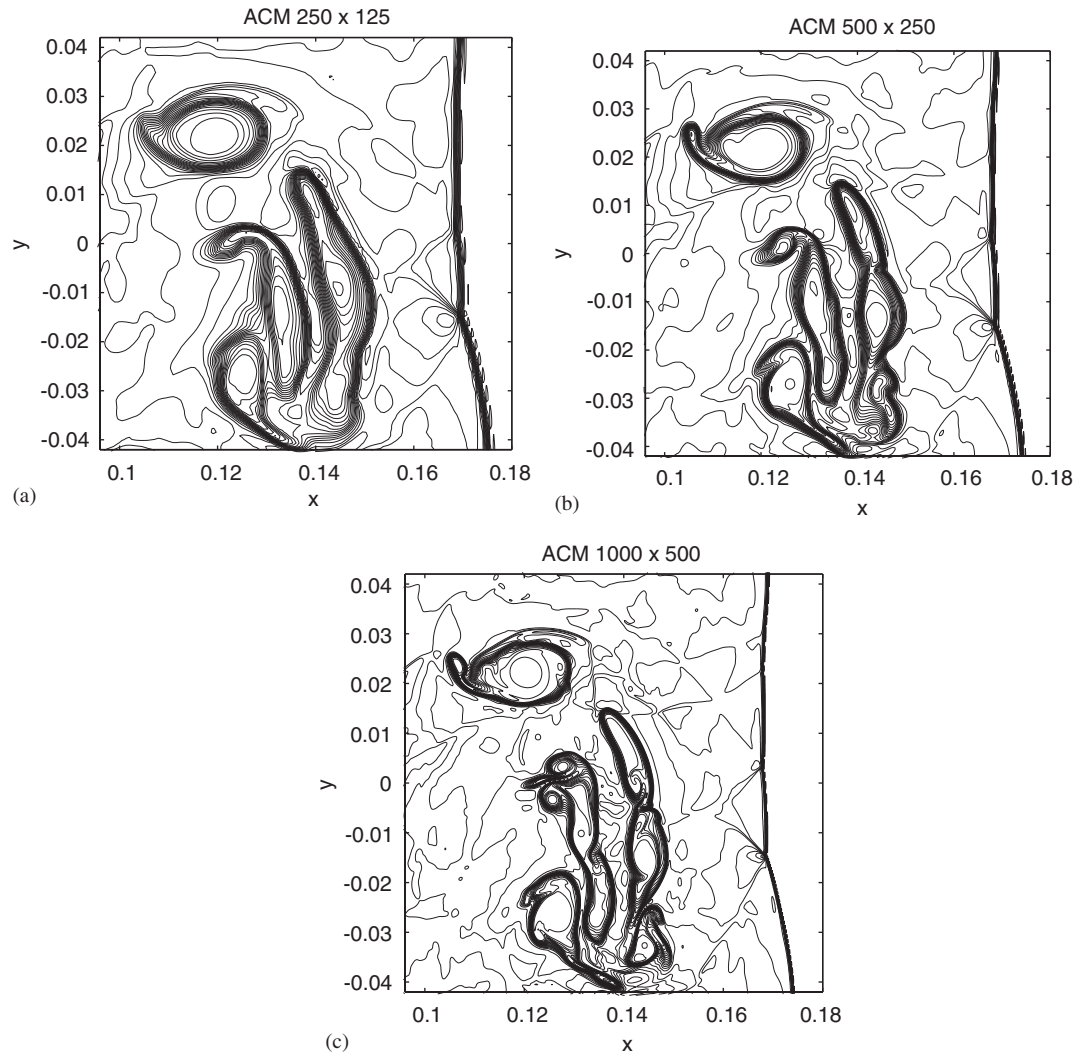

Figure 9. Grid refinement of ACM66-RK4: Density contours at time 125 μs of a planar shock interacting with two initially non-aligned circular hydrogen bubbles: (a) ACM66-RK4, 250×125 grid. (b) ACM66-RK4, 500×250 grid. (c) ACM66-RK4, 1000×500 grid.

between processors is allocated to allow the sometimes wide stencils which occur in high-order difference methods. The computational domain is simple, and the numerical method is explicit, which means that it is easy to obtain good parallel performance. The few global operations, such as determination of the time step, are done through calls to reduction routines in MPI.

Computation times ranged from a few minutes on 10 processors for the smallest problem to as much as 18 h of computing time on 256 processors for the largest computations (two

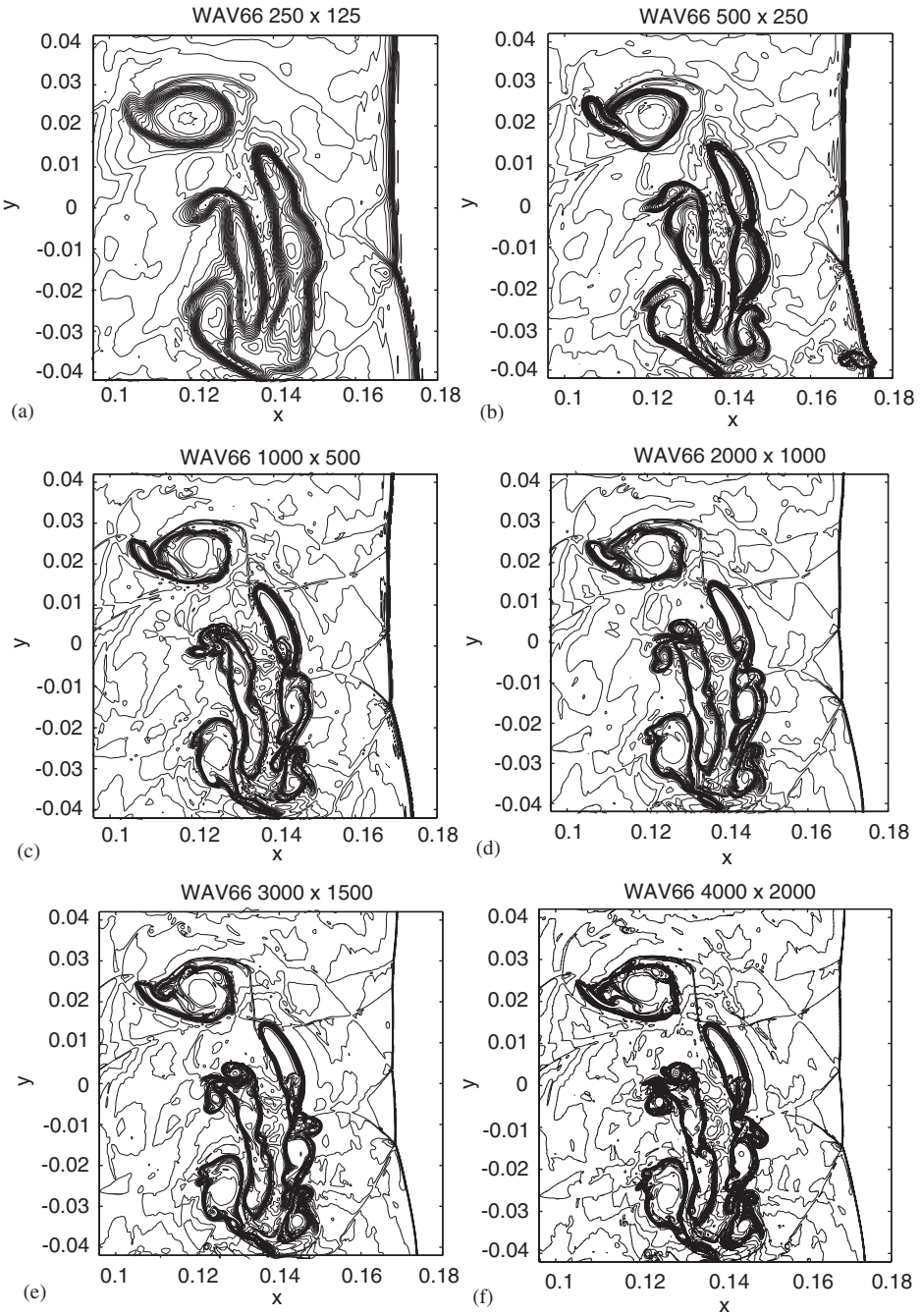

Figure 10. Grid refinement of WAV66-RK4: Density contours at time 125 μs of a planar shock interacting with two initially non-aligned circular hydrogen bubbles: (a) WAV66-RK4, 250×125 grid. (b) WAV66-RK4, 500×250 grid. (c) WAV66-RK4, 1000×500 grid. (d) WAV66-RK4, 2000×1000 grid. (e) WAV66-RK4, 3000×1500 grid. (f) WAV66-RK4, 4000×2000 grid.

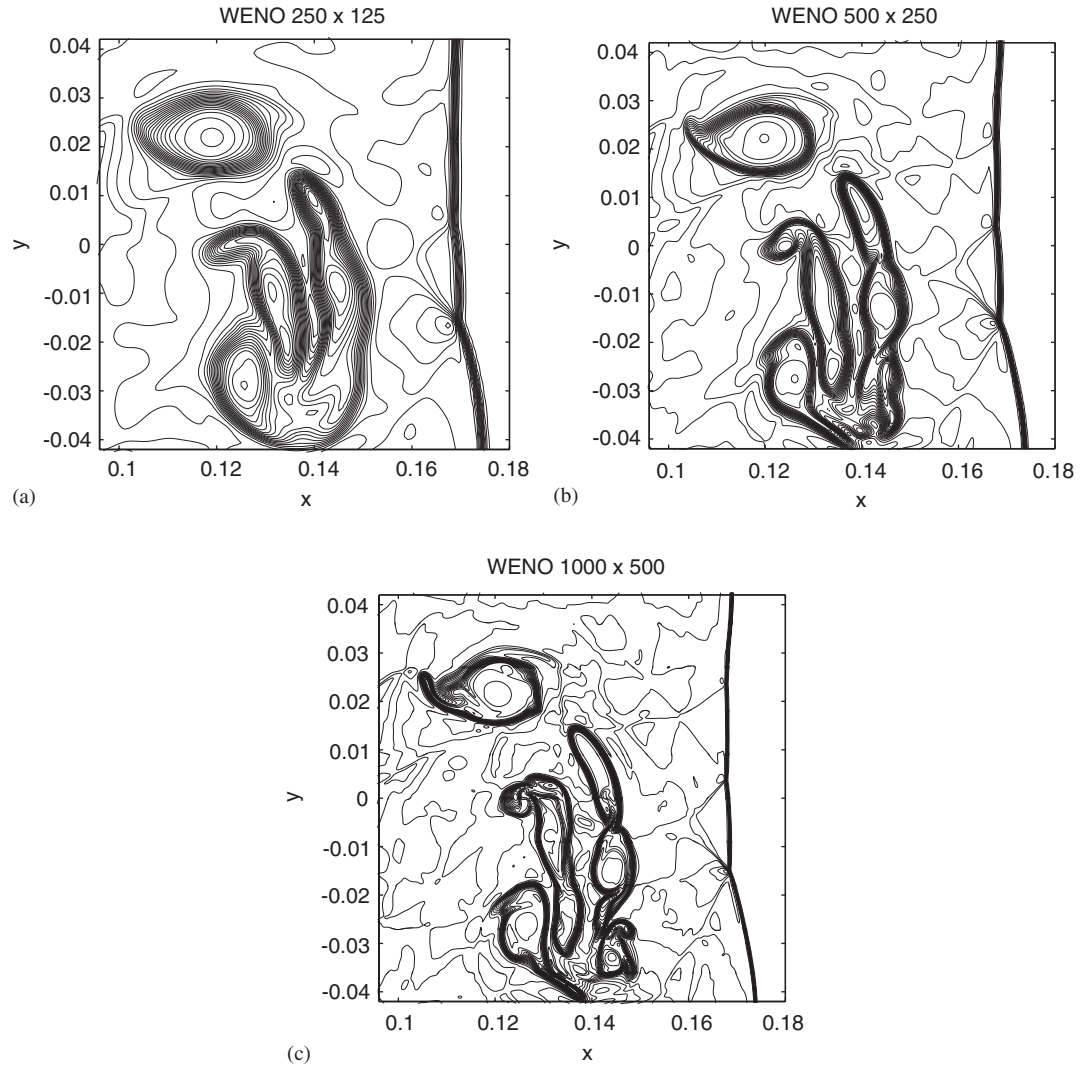

Figure 11. Grid refinement of WENO5-RK4: Density contours at time 125 μs of a planar shock interacting with two initially non-aligned circular hydrogen bubbles: (a) WENO5-RK4, 250×125 grid. (b) WENO5-RK4, 500×250 grid. (c) WENO5-RK4, 1000×500 grid.

bubble case using WAV66-RK4 on a 4000×2000 grid). The different numerical methods were implemented with some care to have an efficient computation. For the WENO5 scheme, the number of operations in our implementation was approximately the same as the number given in Reference [15]. The computational times were as follows. The ACM66-RK4 method had approximately the same CPU time as the second-order TVD scheme (TVD-RK2). The wavelet version of the filter (WAV66-RK4) required almost the same CPU time as the original ACM66-RK4 scheme. The WENO5-RK4 scheme consumed 2.5 times the CPU time of the

TVD-RK2. The measured times are for computing one time step, and the total number of time steps required to reach the same physical time by each method has not been taken into consideration. The number of flux evaluations differ, since the WENO5-RK4, ACM66-RK4 and WAV66-RK4 schemes are integrated by a four-stage fourth-order Runge–Kutta method (i.e. four viscous and inviscid flux evaluations), while for the TVD-RK2 schemes, the fluxes are only evaluated twice by the second-order Runge–Kutta time integrator. The wavelet filter leads to a difference operator which has a stencil width which increases rapidly as the number of multiresolution levels of the wavelet increases. In the present implementation, the number of wavelet levels is small, and a sufficient interprocessor overlap is made. It is, however, possible to implement the wavelet algorithm more generally with an FFT-like butterfly communication pattern. This is a topic of current investigation.

The efficiency of the filter can be improved by not computing the filter terms when the sensor is equal to zero. Due to the complexity in programming, this was not implemented, though it could give some further CPU speedup for the ACM66-RK4 and WAV66-RK4 schemes.

5. CONCLUSIONS

Numerical experiments indicate that the ACM66-RK4 and WAV66-RK4 are less diffusive than WENO5-RK4, and at a computational cost which is only 40% of the cost of the WENO scheme. In comparison with a conventional second-order TVD method, the highly accurate methods exhibit similar results, but with a coarser grid. For the present combustion model, it is difficult to judge whether the solutions are fully resolved. Large-scale structures seem to have converged, but the fine-scale structures seem to be beyond the reach of today's supercomputers without the use of efficient and reliable dynamic grid adaptations. To reduce the grid size while still obtaining well-resolved simulations, a more relevant comparison for the application of practical computations is to incorporate the dual purpose adaptive property of the wavelet sensor, namely, grid adaptation and dynamic numerical dissipation control indicator. We believe that the dual purpose adaptive property of the wavelet sensor is very useful for rapidly developing multiscale problems. This is a topic of current investigation.

ACKNOWLEDGEMENTS

The authors would like to thank Wai Sun Don for providing his spectral chemical reaction code as a guide to build our research code for the supersonic reactive flow study. The generous help from Jahed Djomehri on debugging of the parallel code, and the computer resource support from COSMO on the NASA Ames 512 processor Origin2000 machine are gratefully acknowledged.

REFERENCES

1. LeVeque RJ, Yee HC. A study of numerical methods for hyperbolic conservation laws with stiff source terms. *Journal of Computational Physics* 1990; **86**:187–210.
2. Lafon A, Yee HC. Dynamical approach study of spurious steady-state numerical solutions for non-linear differential equations, Part III: The effects of non-linear source terms in reaction-convection equations. *Computers and Fluid Dynamics* 1996; **6**:1–36.
3. Lafon A, Yee HC. Dynamical approach study of spurious steady-state numerical solutions of non-linear differential equations, Part IV: Stability vs numerical treatment of non-linear source terms. *Computers and Fluid Dynamics* 1996; **6**:89–123.

4. Yee HC, Sweby PK, Griffiths DF. Dynamical approach study of spurious steady–state numerical solutions for non-linear differential equations, Part I: The dynamics of time discretizations and its implications for algorithm development in computational fluid dynamics. *NASA TM*-102820, April 1990; *Journal of Computational Physics* 1991; **97**:249–310.
5. Griffiths DF, Stuart AM, Yee HC. Numerical wave propagation in hyperbolic problems with non-linear source terms. *SIAM Journal on Numerical Analysis* 1992; **29**:1244–1260.
6. Yee HC, Sandham ND, Djomehri MJ. Low dissipative high-order shock-capturing methods using characteristic-based filters. *Journal of Computational Physics* 1999; **150**:199–238.
7. Sjögreen B, Yee HC. Multiresolution wavelet based adaptive numerical dissipation control for shock-turbulence computation. *RIACS Report* 01.01, NASA Ames Research Centre, October 2000.
8. Yee HC, Vinokur M, Djomehri MJ. Entropy splitting and numerical dissipation. *Journal of Computational Physics* 2000; **162**:33–81.
9. Olsson P, Oliger J. Energy and maximum norm estimates for non-linear conservation laws. *RIACS Technical Report* 94.01, 1994.
10. Gerritsen M, Olsson P. Designing an efficient solution strategy for fluid flows. *Journal of Computational Physics* 1996; **129**:245–262.
11. Sandham ND, Yee HC. Entropy splitting for high-order numerical simulation of compressible turbulence. *RIACS Technical Report* 00.10, June 2000. *Proceedings of the 1st International Conference on CFD*, Kyoto, Japan, 10–14 July, 2000.
12. Mallat SG, Zhong S. Characterization of signals from multiscale edges. *IEEE Transactions on Pattern Analysis and Machine Intelligence* 1992; **14**:710–732.
13. Harten A. Multiresolution algorithms for the numerical solution of hyperbolic conservation laws. *Communications in Pure and Applied Mathematics* 1995; **48**:1305–1342.
14. Sjögreen B, Yee HC. Grid convergence of high-order methods for multiscale complex unsteady viscous compressible flows. *RIACS Report* 01.06, April 2001, NASA Ames Research Centre; AIAA 2001-2599. *Proceedings of the 15th AIAA CFD Conference*, Anaheim, CA, 11–14 June, 2001.
15. Jiang G-S, Shu C-W. Efficient implementation of weighted ENO schemes. *ICASE Report No.* 95-73, 1995.
16. Don WS, Quillen CB. Numerical simulation of shock–cylinder interactions. *Journal of Computational Physics* 1995; **122**:244–265.
17. Don WS, Gottlieb D. Spectral simulation of supersonic reactive flows. *SIAM Journal on Numerical Analysis* 1998; **35**:2370–2384.
18. McBride BJ, Heimel S, Ehlers JG, Gorden S. Thermodynamics properties to 6000°K for 210 substances involving the first 18 elements. *NASA SP*-3002, 1963.
19. Svehla RA. Estimated viscosities and thermal conductivities of gases at high temperatures. *NASA Report TR R*-132, 1962.
20. Wilke CR. A viscosity equation for gas mixtures. *Chemical Physics* 1950; **18**:517–519.
21. Harten A. The artificial compression method for computation of shocks and contact discontinuities: III. Self-adjusting hybrid schemes. *Mathematics of Computation* 1978; **32**:363–389.
22. Harten A. On the symmetric form of systems for conservation laws with entropy. *Journal of Computational Physics* 1983; **49**:151–164.